Current Biology, Volume *24*

Supplemental Information

Plume-Tracking Behavior of Flying *Drosophila* Emerges from a Set of Distinct Sensory-Motor Reflexes

Floris van Breugel and Michael H. Dickinson

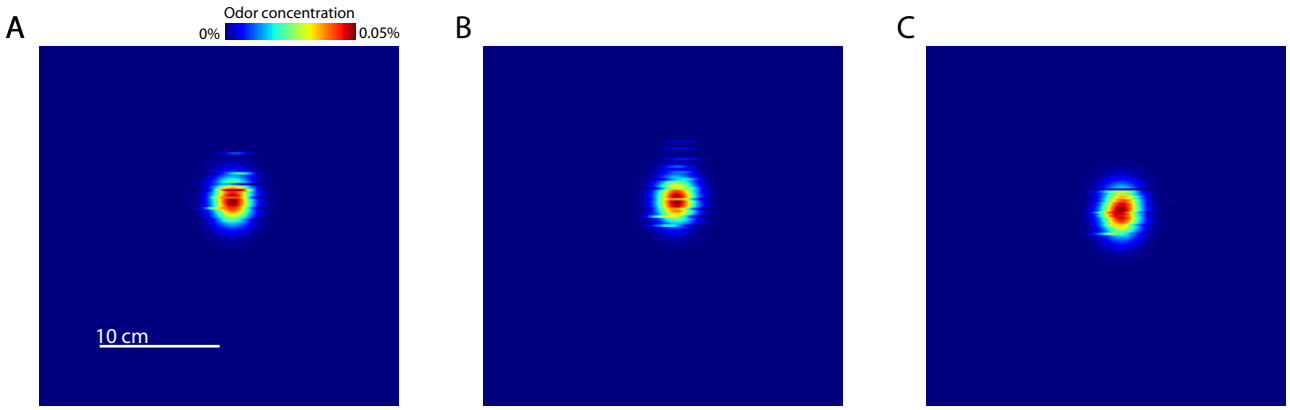

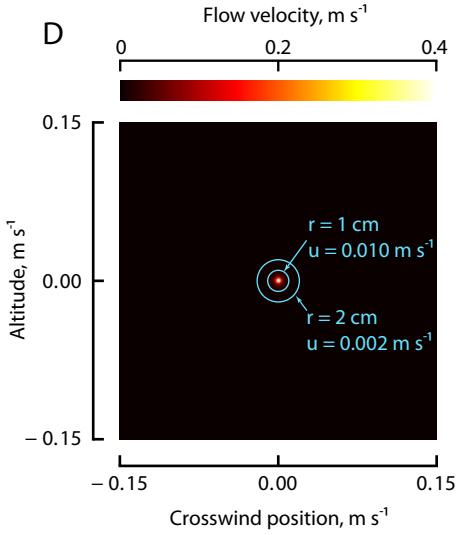

Figure S1. Photo-ionization measurements provide an accurate model of the odor plume throughout the wind tunnel, related to Experimental Procedures.

(A) Gaussian model of the ethanol plume in 0.4 m s^{-1} wind 11 cm downwind from the start of the working section, with the original mean odor concentration measurements (see Figure 1C for an example) used to fit the model superimposed.
(B) Same as A, for measurements made 23 cm downwind from the start of the working section. This panel is repeated from Figure 1D.
(C) Same as C, for measurements made 75 cm downwind from the start of the working section.

As the models in A-C are very similar, we simplified our analysis by using the model from B for the entire length of the wind tunnel, resulting in a cylindrical model of the odor plume (Figure 1). The mean of the error between model B and our PID measurements for the three cross sections were 1.6%, 1.1%, and 3.0% of the peak concentration, respectively.

(D) Photo-ionization detector (PID) suction rate has minimal influence on the fluid flow within the wind tunnel. We modeled the fluid flow due to the suction of the PID (750 mL min^{-1}, tube diameter of 0.6 mm) as a point sink using inviscid flow theory [S1]. The figure shows the magnitude of flow velocities introduced by the point sink centered at (0,0) in the crosswind plane of the wind tunnel. The model indicates that at 5 mm distance, the fluid velocity due to the PID is less than 10% of the ambient wind velocity (0.4 m s^{-1}).

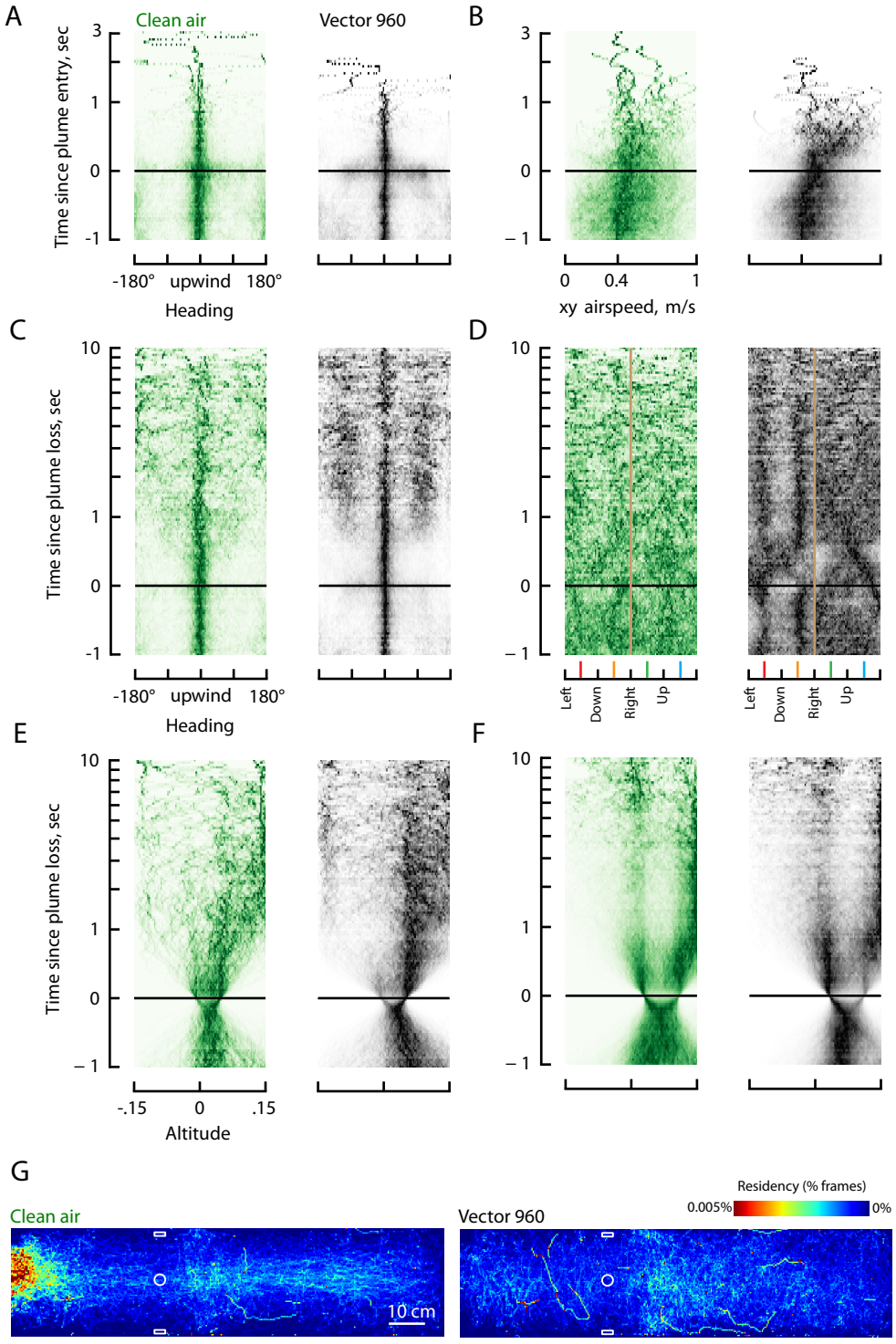

Figure S2. Behavioral responses to a plume of ethanol and Vector960 (fruit fly attractant) are qualitatively similar, related to Results.

(A) Surge heading, see Fig 3B.
(B) Surge airspeed, see Fig 3C.
(C) Cast heading, see Fig 4B.
(D) Cast heading in crosswind plane, see Fig 4C.
(E) Altitude response with checkerboard floor, see Fig 6A.
(F) Altitude response with low contrast floor and dots, see Fig 6B.
(G) Residency heat map, see Fig 6E. Note that although flies in both clean air and Vector 960 explore the visual features, the relative proportion of flies exploring the visual features compared to other portions of the arena in the presence of Vector 960 is much greater.

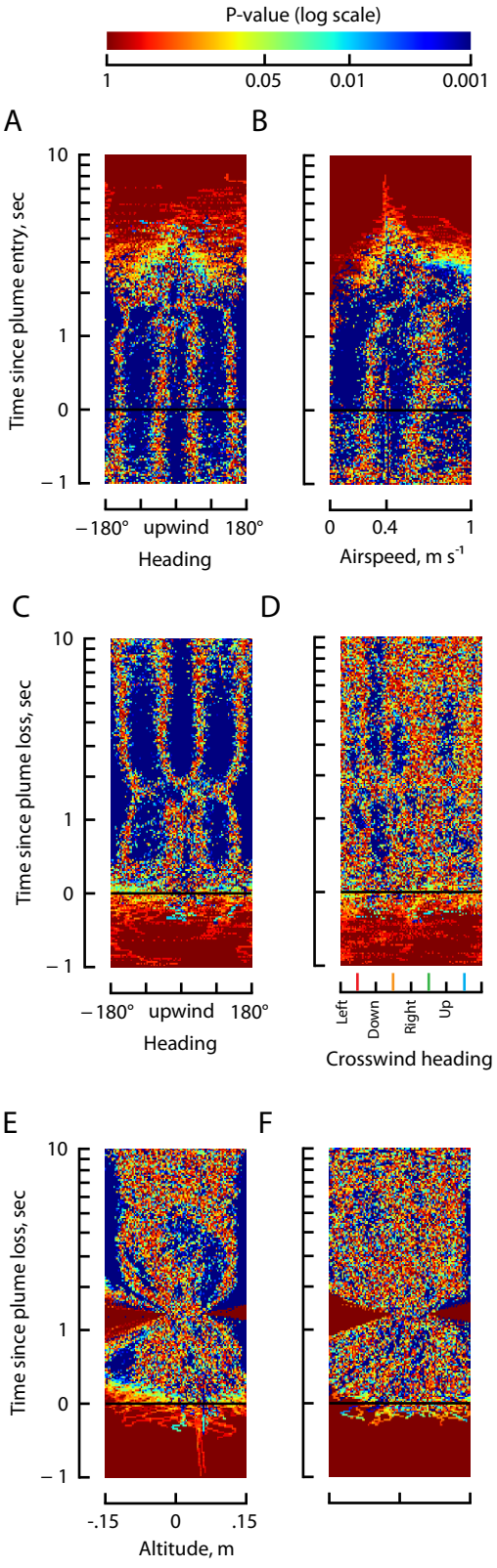

Figure S3. The visibly obvious results presented in Figs 3, 4, 6 are statistically significant, related to Results.

Each panel shows a heat-map (log color scale) representation of the per-pixel p-values that describe the probability that the differences in behavior that we observed in the presence of ethanol vs. clean air are due to random sampling. P-values were calculated by Fisher's exact test, a non-parametric permutation test. See Experimental Procedures for details.

(A) Surge heading, see Fig 3B.
(B) Surge airspeed, see Fig 3C.
(C) Cast heading, see Fig 4B.
(D) Cast heading in crosswind plane, see Fig 4C.
(E) Altitude response with checkerboard floor, see Fig 6A.
(F) Altitude response with low contrast floor and dots, see Fig 6B.

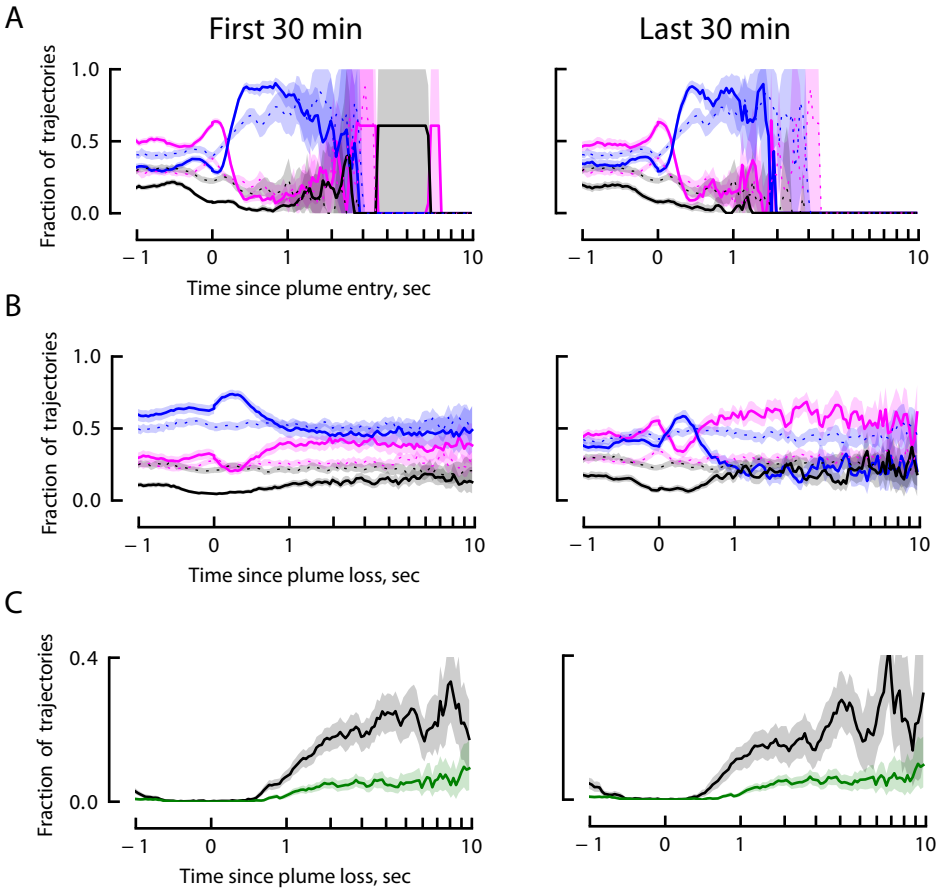

Figure S4. Surge, cast, and object saliency behaviors do not diminish over time, related to Results.

(A) Surge behavior, plotted in the same manner as Fig 3D for trajectories collected in the first 30 minutes of the experiment (left), and the last 30 minutes of the experiment (right).
(B) Casting behavior, plotted in the same manner as Fig 4D.
(C) Visual saliency behavior, plotted in the same manner as Fig 6E.

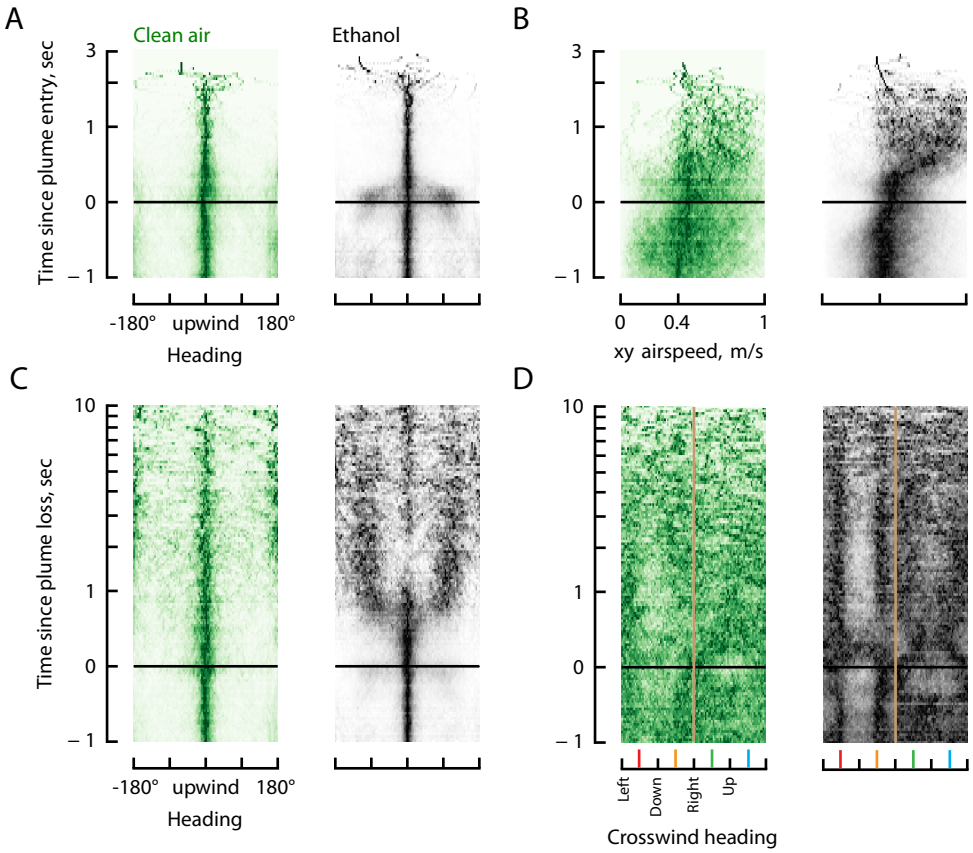

Figure S5. Cast and surge behaviors are qualitatively similar in the presence of a high contrast checkerboard floor and a low contrast floor with high contrast spots, related to Figure 6.

After performing the experiments described in Fig 6, we repeated the analysis presented in Figs 3-4 with our data collected with the visual environment shown in Fig 6B. We did not find any qualitative difference.

(A) Surge heading, see Fig 3B.
(B) Surge airspeed, see Fig 3C.
(C) Cast heading, see Fig 4B.
(D) Cast heading in crosswind plane, see Fig 4C.

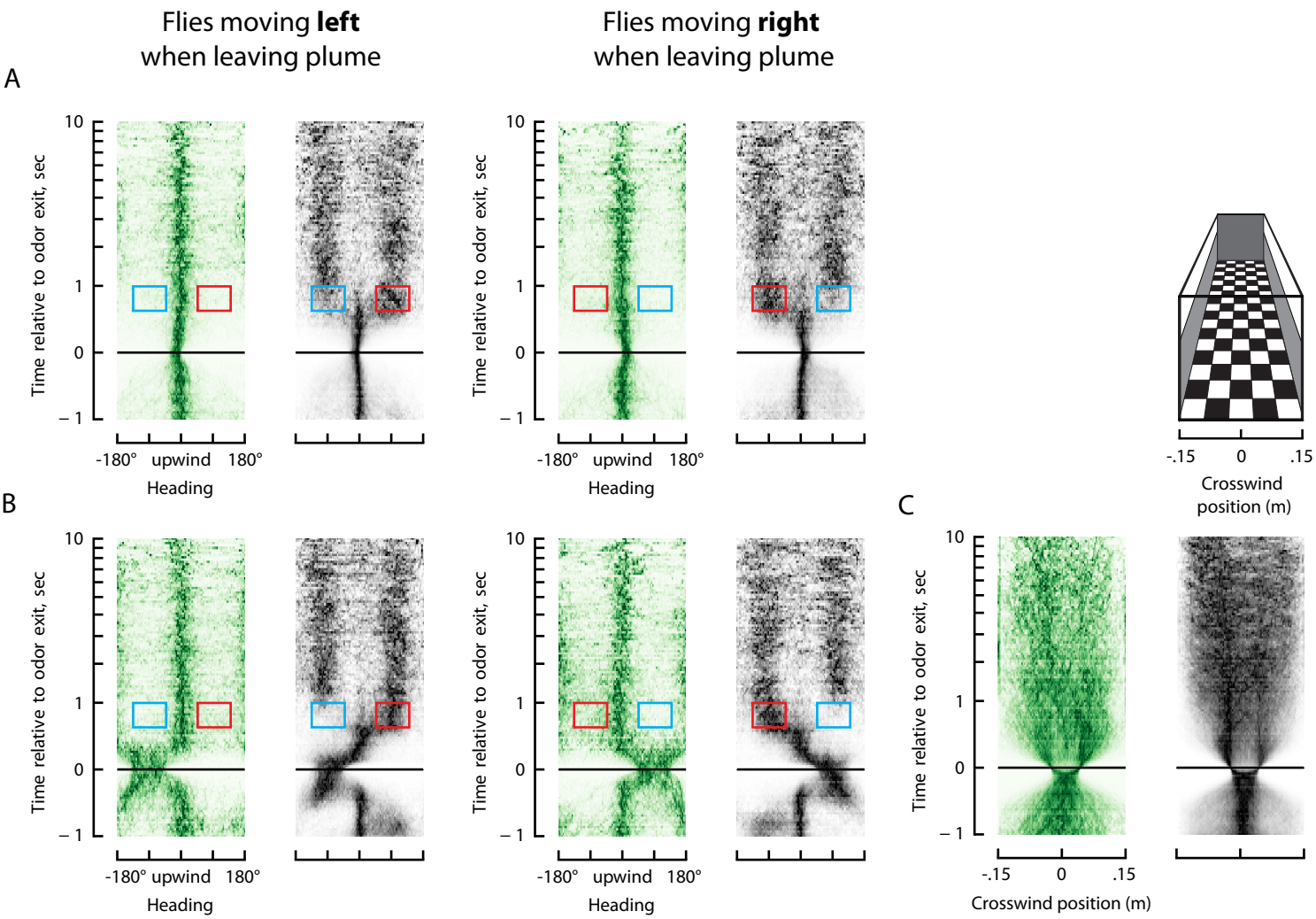

Figure S6. In a constrained environment, flies casting initiation is likely mediated by visual expansion cues, related to Discussion.

(A) Casting behavior, plotted as in Figure 4B, for flies that left the odor plume with a heading between ±10° and ±20°. Calculating the ratio of the sum of the distribution in the regions outlined in red, and the sum of those outlined in red and blue indicates that flies were 56% more likely to initiate casting in the direction opposite their departure heading. This result was not, however, significant when compared to the control data ($p>0.4$, Fischer's exact test).
(B) Same as A, however for flies that left the plume with headings between ±45° and ±135°. In this case, flies were 69% more likely to initiate casting in the direction opposite their departure heading. These results are also not statistically significant compared to controls ($p>0.4$, Fischer's exact test).
(C) Crosswind position of flies relative the time they left the odor plume, plotted in a similar manner to 4B.

Table S1. Detailed statistics of our trajectories under the different experimental conditions, related to Results.

				Clean air control				**Odor stimulus**				
Visual pattern	**Wind speed (m/s)**	**Odor**	**# Exps (# Flies)**	***# Trajecs***	***Mean length (mean ±std) (sec)***	***# Trajecs found plume***	***# Odor encounters per trajec (mean±std)***	**# Trajecs**	**Mean length (mean ±std) (sec)**	**# Trajecs found plume**	**# Odor encounters per trajec (mean±std)**	**Figures**
Checkers	0.4	Ethanol	9 (108)	3743	5.3±4.4	1368	1.5±1.0	5542	7.6±8.4	3182	3.0±3.0	2ADE; 3A-F; 4A-F; 5A; 6A-B
Stripes ∥ wind	0.4	Ethanol	3 (36)	1136	6.5±6.0	313	1.4±0.9	1425	5.1±4.4	609	2.0±1.4	3E; 4E
Stripes ⊥ wind	0.4	Ethanol	3 (36)	1082	5.2±4.6	315	1.5±1.2	929	6.7±6.4	497	2.4±1.9	3E; 4E
Dots	0.4	Ethanol	5 (60)	2508	5.6±5.2	1090	1.8±1.7	2705	7.4±7.5	1795	3.0±2.9	5B-D; S5
Checkers	0.3	Ethanol	5 (60)	5453	5.4±5.5	1158	1.6±1.1	4509	6.3±6	2606	3.4±3.6	3F; 4F; 6B
Checkers	0.6	Ethanol	5 (60)	1400	5.4±4.7	433	1.4±0.9	2137	10.2±12.2	1056	3.2±2.7	3F; 4F; 6B
Checkers	0.4	Vector960	4 (48)	2819	6.0±5.3	888	1.7±1.3	3185	6.8±6.5	1635	2.2±1.9	S2
Dots	0.4	Vector960	7 (84)	5732	6.1±5.0	3879	2.1±1.7	4619	6.3±5.0	3580	2.7±2.3	S2
Checkers	0.4	Pulsing Ethanol	4 (48)	3417	6.6±6.8	1036	1.5±1.0	1421	6.4±7.0	173	1.2±0.8	2D,E

Supplemental experimental procedures

Animals

Experiments were performed on 2-to 3-day-old fruit flies, *Drosophila melanogaster* Meigen, Heisenberg/Canton-S background. Flies were deprived of food, but not water, for 6-8 hours prior to the start of the experiment in order to motivate flight. Flies were on a 16:8 hr (light:dark) cycle, with lights out at 11pm local time. For each experimental trial, we introduced a group of 12 female flies to the corner of the arena within a small test tube between 6 and 8 pm. The flies were then free to move throughout the flight arena for a period of 12-18 hours, during which time data were collected automatically.

Flight arena

We performed all experiments in a 1.5 x 0.3 x 0.3 m working section of a wind tunnel (Figure 1A) that has been described previously [S2–S5]. In these experiments, except where otherwise noted, the wind tunnel was set to 0.4 m s^{-1}, which was chosen based on previously published measurements of wind levels in an orange orchard [S2]. On the two long walls and floor of the arena we projected different visual stimuli using a Lightspeed Designs DepthQ (Oregon City, OR) projector with the color wheel removed (120 Hz update rate, 360 Hz framerate, mean luminance of 50 cd/m^2). We generated the stimuli using the VisionEgg open-source image-rendering software [S6]. For the purposes of tracking, the arena was backlit with an array of near-infrared (640 nm) LEDs. The cameras were equipped with long-pass filters (Hoya R-72) so that the camera images were not contaminated by the pattern that was displayed in visible wavelengths.

We tracked the 3-dimensional position of individual flies within the chamber using a camera based real-time tracking system that is described in detail elsewhere [S7]. The 10-camera (Basler Ace 640-100 gm, Basler, Exton, PA) system generated an estimate of fly position at 100 frames per second with a median latency of 39 ms by triangulating the fly's position from 2-dimensional tracking data contributed by two or more synchronized cameras. The 3-dimensional position was estimated with an extended Kalman filter, using a constant velocity motion model. Because of the high frame rate relative to flight behavior, we found that this simplification worked well in practice. The resulting trajectories were smoothed to remove digitization errors and to estimate velocity, using a simple forward/reverse, non-causal Kalman filter. We excluded non-flying trajectories, as well as trajectories that were less than 1 second in length, from our analysis.

Odor stimulus

In previous studies, apple cider vinegar or a banana and yeast cocktail have been used to attract flies [S2, S8–S10]. These odors are complex mixtures of compounds with different volatilities, making contamination an issue when delivering pulsed stimuli. To circumvent this issue we chose to use pure ethanol, a common component of rotting fruit, which adheres much less to tubes and other parts of the wind tunnel, and is quite attractive to flies [S11–S14]. To confirm that the behaviors we observed were due to the detection of an attractive odor, rather than physiological changes due to our choice of ethanol, we repeated our experiments with the commercially available fruit fly attractant similar to balsamic vinegar, Vector960 (Pest Control Solutions, St. Louis, MO). Although the responses were less obvious (likely due to differences in concentration in the air), we did not find any qualitative differences (Figure S2). Between switching odors, we thoroughly cleaned all the potentially contaminated tubes and vials with hexane, and ran the experiment with no odor to ensure that all the system was clean of any residual odors.

Odor delivery

To compare the responses of flies to an attractive odor plume and clean air we developed a controlled odor delivery system (Figure 1B). Breathable compressed air (Praxair, Seattle, WA) was sent through a

mass flow controller (902C-P5BM-I1, Sierra Instruments, Monterey, CA) at 158 sccm. We used an Arduino Nano and solid-state relay to switch a three-way solenoid valve (LHDA0531215H, Lee Corp, Essex, CT) that directed the airflow either through an aquarium stone submerged in liquid ethanol contained in a glass vial, or through uncontaminated tubes. These two pathways passed through another 3-way solenoid valve controlled in parallel with the first, such that the desired flow of either odorous air or clean air entered the wind tunnel through a 1.67 mm (I.D.) Polyethylene tube from the same point with minimal switching latency.

For pulsing experiments, the Arduino was programmed to switch the odor on for 0.4 seconds, allowing clean air to pass through the system between each pulse. The timing of the pulses was sent over USB to the computer and saved to disk for analysis. For the constant plume experiments, the odor delivery was turned on at midnight, and persisted for 4 hours, after which time the solenoids were switched off to deliver clean air for the remainder of the night.

Odor plume calibration

To determine the three-dimensional odor landscape we scanned the wind tunnel with a miniature photoionization detector (PID) (200B miniPID, Aurora Scientific, Ontario, Canada) in the presence of an ethanol plume. The suction rate of the PID was set to the minimum value of 750 mL min^{-1}. We confirmed that the suction had minimal effects on the fluid flow within the wind tunnel using inviscid flow theory (Figure S1). To scan the pulsing plume, we positioned the PID at one point and saved the time course of the Arduino's control signals together with the output of the PID. We repeated these measurements for 28 pulses at each of 61 positions, and constructed a 3-dimensional time-varying Gaussian model based on the data using a least squares fit. Because we focused our analysis on the results collected with the continuous plume, rather than the pulsing plume, the results from these measurements are not shown for lack of space.

To calibrate the continuous plume, we attached the PID system to a frame that was actuated with a stepper motor and timing belt. The motor was controlled so that the PID was driven at 0.01 m s^{-1} back and forth along the horizontal crosswind direction through the plume for a period of 15 minutes (50 round trips), while streaming the data. This was repeated for 12 different altitudes, each at three different positions along the wind line. For each run we calculated the baseline subtracted mean (e.g. Figure 1C), and used these means calculate a least squares fit to a two-dimensional Gaussian model of the crosswind concentration profile at each of the three positions along the wind line at 11, 23, and 75 cm from the upwind end of the working section (Figure 1D). The three fits were very similar, so to simplify our analysis we modeled the odor plume as a constant Gaussian 2D model that stretched down the length of the wind tunnel as a cylindrical plume. This 2D Gaussian model, based on the measurements taken at 23 cm downwind from the upwind end of the working section, yielded mean errors for the three positions of 1.6%, 1.1%, and 3% of the peak concentration, respectively. To compare flies' odor plume tracking behavior under different wind speed conditions, we repeated the entire calibration process for three wind speeds (0.3, 0.4, and 0.6 m s^{-1}). For the slowest wind speed, we reduced the mass flow of air to 77 sccm to obtain a stable plume. The mass flow rates for 0.4 and 0.6 m s^{-1} wind speeds were both 158 sccm.

The photo-ionization detector provides data in arbitrary units, which must be calibrated in order to provide a measure of the actual odor concentration. Unfortunately, the calibration shifts significantly over the course of a few hours. Since each calibration routine took over 6 hours, we took a first principles approach to calibrate the magnitude of the odor signal. We assume that by bubbling air through ethanol, the ethanol and air mixture in the vial is at steady state. This assumption potentially yields an overestimate of the concentration of ethanol. Under this assumption, the mole fraction of ethanol in the air is described by the ratio of the vapor pressure of ethanol to the atmospheric pressure:

$$Mole\ fraction\ of\ ethanol = \frac{6.66\ KPa}{101.325\ KPa} = 0.065.$$

Given the mass flow rate of air through the system, 158 mL m^{-1}, we calculate the flow of moles of ethanol per minute using the ideal gas law:

$$n = \frac{PV}{RT} = \frac{(101325\ Pa)(0.000158\ m^3)}{(8.314\ J\ K^{-1}mol^{-1})(293.15\ K)} = 0.00656\ moles\ air/min,$$

$$moles\ ethanol/min = 0.00656 * 0.065 = 4.26x10^{-4}.$$

The wind speed in the wind tunnel was set to 0.4 m s^{-1}, or 24 m min^{-1}, thus over the course of one minute, $4.26x10^{-4}$ moles of ethanol are distributed across 24 meters along the wind direction, or $1.775x10^{-5}$ moles m^{-1}. The 2-dimensional Gaussian model from our PID measurements describes the concentration profile in the plane perpendicular to wind direction. Normalizing the Gaussian model such that its integral is $1.775x10^{-5}$ yields a function that describes the moles of ethanol in a $1 \cdot dy \cdot dz$ m^3 volume. Using the ideal gas law again, we can calculate the number of moles of total gas in that same volume (41.57 moles). Thus, to calculate the molar fraction of ethanol at any point in the wind tunnel we take the ratio of the output from the normalized Gaussian function and 41.57. This yields a peak concentration of 0.0476% moles of ethanol in clean air.

Trajectory reconstruction and analysis

By combining the three-dimensional trajectories from our tracking system with our model of the odor landscape we were able to reconstruct each flies' olfactory experience synchronized to its behavior. Visual inspection of the trajectories indicated that in the presence of both the pulsing and continuous odor plumes, the flies were casting and surging as has been described previously (Figure 1E-G). To uncover the details of this behavior, we developed a custom analysis that allowed us to present the results of all of the trajectories together. All our analysis code was written in Python using the open-source software packages Scipy and MatPlotLib.

The tracking software used to collect the 3-dimensional flight trajectories was unable to maintain the identity of individual flies over the entire course of our experiments (12-18 hours). Therefore, we were unable to test whether individual flies behaved consistently different from one another, and each trajectory was treated as an independent sample. The values of "N" reported throughout the figures in this paper represent the number of trajectories that contributed data to each figure panel. This, however, is only one interpretation of "N". In many cases, individual trajectories contributed more than once to our analysis, if the fly entered and left the odor plume multiple times. Furthermore, the number of trajectories should not be confused with the number of animals (which range between 36 and 108 per experiment). These alternate values of "N" are reported in a supplementary Table S1.

Estimation of delays in Figs 3, 4

To estimate the delay in surge and cast behavior, we first assumed that this value would be Normally distributed. In this case, our behavioral observations reported in Figs 3D and 4D should follow a cumulative distribution function (CDF) of the Normal distribution. For Fig 3D, we used least squares to fit the CDF to the fraction of flies flying upwind between 0-400 ms after entering the plume. For Fig 4D we used least squares to fit the CDF to the fraction of flies flying crosswind between 10-1100 ms after leaving the plume.

Statistics – comparison of in Figs 3, 4

To compare the distributions of upwind and crosswind headings in Figs 3F-G and 4F-G we calculated a "distribution concentration" value for each sensory manipulation. For surge behavior, as in Fig 3F-G, this value was defined as the difference between the peak value and the integral between upwind and 45° in the Ethanol response – Control response distribution (Fig 3Fii, Gii). In both cases, the differences in distribution concentrations for different visual and wind conditions were significant ($p \leq 0.001$, Fischer's exact test). For casting behavior, as in Fig 4F-G, we calculated the distribution concentration as the

difference between the peak value and the integral between 45° and 135° in the Ethanol response – Control response distribution (Fig 4Fii, Gii). The differences in distributions of Fig 4Fii were significant ($p \leq 0.001$, Fischer's exact test), whereas the differences in the distributions of Fig 4Gii were only significant for the low wind case.

Statistics – Fisher's exact test

To determine which aspects of flies' behavior were due to the presence of an attractive odor, we compared their behavior in the presence of an attractive odor plume to their behavior in the presence of a pseudo-plume of clean air. We found several elucidating behavioral parameters that showed clear differences between the two treatments, including flight heading in the horizontal and vertical planes, airspeed, and altitude. Rather than reducing the data to a single descriptive statistic, we developed a method whereby we could assign a p-value to each individual pixel of the density maps shown in Figures 3,4 and 6 (Figure S3). These p-values give a quantitative statistical sense of the importance of the behavioral differences between the clean air and attractive odor cases. To determine these p-values, we used a non-parametric resampling approach, Fisher's exact test [S15, S16]. For each resampling, we randomly reshuffle the labels "clean air" and "attractive odor" assigned to the trajectories, resulting in two new test groups. These new groups are run through our analysis, resulting in density maps (eg. Figure 3B). Each row of the density maps is normalized such that the integral for that row equals one. Next, we calculated the differences between the two groups and record this value on a pixel-by-pixel basis. After repeating this process for 1000 resamplings, we can construct a distribution of these differences for each pixel. Comparing the difference between the actual control and attractive odor cases to this distribution allows us to calculate a two-tailed p-value that describes the probability that our result is due to the random sampling process, rather than an actual difference in the underlying mechanisms driving the behavior. Larger numbers of resamplings provide more resolution, and confidence, on the p-value. The computations involved in resampling data at the trajectory level, and calculating p-values on a per pixel basis, are not trivial. We found that 1000 resamplings gave consistent results while providing sufficient resolution to calculate p-values as small as 0.001. All of the clear behavioral differences we present in this paper are significant, in the statistical sense, with p-values of 0.001-0.01 across the relevant time and parameter space (Figure S3).

Statistics - bootstrapping

Many of the analyses presented in this paper rely on the distributions (D*) of behaviors observed in large numbers of trajectories to draw conclusions on flies' stereotypical behavior. In order to provide a sense of variability in our data due to random sampling processes, we used a basic non-parametric bootstrapping method to calculate 95% confidence intervals for these distributions [S17]. The general approach is to resample the original set of trajectories (Y), with replacement, to obtain a new set of trajectories (Y*), with the same or similar sample size as the original dataset. Note that Y* may include duplicates. Then the analysis is performed on Y* to determine the distribution D*. This is repeated many times, and the resulting values of the distributions D* are sorted so that a mean and 95% confidence interval can be calculated. In our analysis, we found that 500 iterations provided repeatable measures of confidence intervals. For a more detailed explanation, including several examples, see [S18].

Model

In order to quantitatively assess the importance of the three sensory-motor reflexes we describe, we created a simple 3-dimensional simulation. We ran the simulation under two conditions: (1) a single visual feature that emitted a static cylindrical plume 6 cm in diameter; (2) a single visual feature that randomly emitted 6 cm diameter spherical "packets of attractive odor at a mean rate of 8 per second. We reasoned that these simplified models (as opposed to modeling actual aerodynamics) would be sufficient to explore the implications of flies' plume tracking behavior because their olfactory experiences are largely determined by their own flight dynamics. The values were chosen arbitrarily such that the plume-

tracking problem would be difficult, but not impossible. Different values resulted in consistent behavioral differences between the tracking algorithms we tested. The odor packets were advected by a 0.4 m s^{-1} wind. For the simulation with spherical packets, the wind randomly changed direction according to a uniform distribution between ±100°/second. This resulted in a slow random walk of wind speed direction. Once the first odor packet reached a distance of 1 meter from the source, a virtual fly was spawned inside of that odor packet. This allowed us to circumvent the problem of initial plume finding, which is beyond the scope of this study. In the simulation with a constant cylindrical plume, the flies were spawned 1 meter from the source, with a random position inside the plume.

The virtual fly was programmed to surge and cast with the same sensory-motor delays we observed (190 ms, and 450 ms, respectively). To simplify programming, we allowed the virtual fly to have access to the absolute wind direction, rather than implementing the programmatically more complex solution of visual anemotaxis. Our experiments did not provide accurate insight as to how flies trigger casting reversals, either in the horizontal or vertical directions. For our model, we initially chose 0.5 second casting intervals for both the horizontal and vertical aspects of casting (these values are similar to what we observed for flies in our wind tunnel, Figure S6). However, we quickly noted that by using an identical reversal frequency for horizontal and vertical casts, the virtual flies would follow a highly periodic (X-shaped) pattern in the crosswind plane. Whereas this strategy may be ideal in the case of a pulsing plume in constant wind, following this algorithm in randomly shifting (or turbulent) winds could prevent a fly from ever re-locating the plume because the plume may have shifted outside of the flies periodic search trajectory. In this case, a more strategic algorithm may be to use a less periodic trajectory, accomplished by adding a noisy element to the reversal timing, or by using an irrational relationship between the horizontal and vertical cast timing. For our simulation, we arbitrarily chose 0.5 second for the horizontal reversals, and 0.3090169 seconds for the vertical reversals. Note that with these values, the ratio of horizontal to vertical casting periods is approximately equal to the golden ratio, an elegant irrational number found throughout nature and art [S19]. This was an arbitrary choice, and future experiments will be necessary to determine what ratio of horizontal to vertical casting periods flies use, and whether this value changes under different environmental conditions (e.g. wind and visual). Although our simulation provides the framework for exploring what values may be theoretically optimal under different conditions, without a biological basis for environmental conditions and behavioral actions we are hesitant to draw any conclusions.

Due to the sensory-motor delays and the assumption of symmetric casting behavior, the virtual flies began casting around a point that that was offset from the last point of odor contact, reducing their chances of re-encountering the plume. This was inconsistent with our observations, which appear to suggest that flies' casting is, on average, centered about the plume (Figs 2A, 4A). To correct for this, we adjusted the timing of the first casting reversal to take into account the delays. This is a key assumption that needs to be tested in animals: do flies, and other insects, center their casting about the point of last encounter, or about the point of casting initiation? Testing this question requires doing experiments in an arena where casting reversals are primarily internally triggered, rather than being visually influenced. Because of the narrow geometry of our wind tunnel, we could not address this point with our dataset.

Once the fly came within 20 cm of the visual feature, we programmed it to approach the feature, and if it sensed an odor, land on it. The 20 cm choice was again arbitrary, and will likely depend on the size, and contrast, of the actual feature. We allowed each simulation to run for 30 seconds, after which time flies had typically either landed on the feature, or moved past it without hope of relocating it.

We ran four simulations with different behavioral algorithms (each with 1000 repetitions), in the two plume conditions (constant, pulsating). In the first, the virtual fly followed the algorithm outlined above (similar to what we observed real flies do). Next, we set the surge and cast delays to be equal (190 ms), and found that the time flies required to locate the food source increased in the presence of both the constant and pulsatile stimuli. Next, we set both the surge and cast delay to zero, and found that under these conditions the time to localization decreased for the constant plume case, but increased for the pulsatile case. Finally, we removed the visual attraction component, and found that nearly none of the flies successfully located the source (due to the sensory-motor delays, which put flies off-course) for both the constant and pulsatile stimuli. Although simple, our simulation allows for easy comparisons of

different behavioral and environmental parameters. We invite other researchers to explore this space using our code, which is made freely available here: *https://github.com/florisvb/FlyPlumeTracking*.

Supplemental References

S1. Batchelor, G. K. (1967). An Introduction to Fluid Dynamics (Cambridge University Press).

S2. Budick, S. A., and Dickinson, M. H. (2006). Free-flight responses of *Drosophila melanogaster* to attractive odors. J. Exp. Biol. *209*, 3001–17.

S3. Maimon, G., Straw, A. D., and Dickinson, M. H. (2008). A simple vision-based algorithm for decision making in flying *Drosophila*. Curr. Biol. *18*, 464–70.

S4. Straw, A. D., Lee, S., and Dickinson, M. H. (2010). Visual control of altitude in flying *Drosophila*. Curr. Biol. *20*, 1550–6.

S5. Van Breugel, F., and Dickinson, M. H. (2012). The visual control of landing and obstacle avoidance in the fruit fly *Drosophila melanogaster*. J. Exp. Biol. *215*, 1783–98.

S6. Straw, A. D. (2008). Vision egg: an open-source library for realtime visual stimulus generation. Front. Neuroinform. *2*, 4.

S7. Straw, A. D., Branson, K., Neumann, T. R., and Dickinson, M. H. (2011). Multi-camera real-time three-dimensional tracking of multiple flying animals. J. R. Soc. Interface *8*, 395–409.

S8. Frye, M. A., Tarsitano, M., and Dickinson, M. H. (2003). Odor localization requires visual feedback during free flight in *Drosophila melanogaster*. J. Exp. Biol. *206*, 843–855.

S9. Duistermars, B. J., Chow, D. M., and Frye, M. A. (2009). Flies require bilateral sensory input to track odor gradients in flight. Curr. Biol. *19*, 1301–1307.

S10. Gaudry, Q., Hong, E. J., Kain, J., de Bivort, B. L., and Wilson, R. I. (2013). Asymmetric neurotransmitter release enables rapid odour lateralization in *Drosophila*. Nature *493*, 424–8.

S11. Barrows, W. M. (1907). The reactions of the Pomace fly, *Drosophila ampelophila* loew, to odorous substances. J. Exp. Zool. *4*, 515–537.

S12. West, A. S. (1961). Chemical attractants for adult *Drosophila* species. J. Econ. Entomol. *54*, 677–681.

S13. Reed, M. R. (1938). The olfactory reactions of *Drosophila melanogaster* Meigen to the products of fermenting banana. Physiol. Zool. *11*, 317–325.

S14. Zhu, J., Park, K.-C., and Baker, T. C. (2003). Identification of odors from overripe mango that attract vinegar flies, *Drosophila melanogaster*. J. Chem. Ecol. *29*, 899–909.

S15. Fisher, R. A. (1922). On the Interpretation of $\chi 2$ from Contingency Tables , and the Calculation of P. J. R. Stat. Soc. *85*, 87–94.

S16. Fisher, R. A. (1935). The design of experiments. (Oxford, England: Oliver & Boyd).

S17. Efron, B. (1979). Bootstrap methods: another look at the jackknife. Ann. Stat. *7*, 1–26.

S18. Carpenter, J., and Bithell, J. (2000). Bootstrap confidence intervals: when, which, what? A practical guide for medical statisticians. Stat. Med. *19*, 1141–1164.

S19. Livio, M. (2008). The golden ratio: The story of phi, the world's most astonishing number (Random House Digital, Inc.).